

Modelling Resistive Wall Modes with Self-consistent Inclusion of Drift Kinetic Resonances

Yueqiang Liu 1), M.S.Chu 2), I.T. Chapman 1), C.G. Gimblett 1), M.P. Gryaznevich 1), R.J. Hastie 1), T.C. Hender 1), D.F. Howell 1), S. Saarelma 1) and JET-EFDA contributors*

JET-EFDA, Culham Science Centre, Abingdon, OX14 3DB, UK

1) Euratom/UKAEA Fusion Association, Culham Science Centre, Abingdon, OX14 3DB, UK

2) General Atomics, San Diego, California 92186, USA

*See the Appendix of F. Romanelli et al., paper OV/1-2, this conference

E-mail contact of main author: yueqiang.liu@ukaea.org.uk

abstract. We investigate the effect of drift kinetic damping on the resistive wall mode (RWM), due to the mode resonance with magnetic precession drifts and/or bounce motion of bulk plasma thermal particles. A self-consistent toroidal drift kinetic model is developed and incorporated into the MHD code MARS-F [Y.Q. Liu, *et al.*, Phys. Plasmas **7**, 3681 (2000)]. The new code (MARS-K) is used to study the RWM stability in ITER steady state scenarios, and to model the resonant field amplification (RFA) for JET plasmas. The self-consistent simulations predict a parameter regime where the RWM in ITER is fully stabilised by the drift kinetic effects combined with the toroidal plasma flow. A wider stable parameter space is predicted by the perturbative approach based on the ideal kink mode eigenfunction. The difference is attributed to the modification of the RWM eigenfunction by the kinetic effects. Applying the MHD-kinetic hybrid code MARS-K to JET plasmas leads to the identification of possible instabilities responsible for the observed RFA at lower beta.

1. Introduction

Advanced tokamak scenarios, including those foreseen for ITER, aim at simultaneously maximising the plasma pressure and operating in steady state. This requires that all slowly evolving macroscopic MHD instabilities be stable. It is well known that the resistive wall mode (RWM), which is a global kink-like, non-axisymmetric instability, with growth rates reduced by the surrounding conducting wall(s), poses the limit to the steady state operation of advanced tokamaks. Therefore, it is critical to ensure that this mode stays stable when the plasma pressure exceeds the ideal no-wall beta limit.

Two approaches to stabilise the mode have been under extensive investigation during recent years, namely active control and rotational stabilisation of the mode, with kinetic damping effects being involved. The physics of rotational (or kinetic) stabilisation of the RWM remains unresolved, especially in view of the new experimental evidence from DIII-D [1, 2] and JT-60U [3], where balanced neutral beam injection produces RWM stable plasmas with very slow toroidal flow. Understanding the damping physics of the RWM is of significant importance not only for predicting the critical rotation speed for ITER plasmas, but also for understanding other related physics effects, such as the resonant field amplification (RFA), and plasma momentum damping (one of the momentum damping mechanisms, the neoclassical toroidal viscous damping, depends on RFA).

In this work, we develop a full toroidal drift kinetic model for the RWM, and apply this model to predict the RWM stability in ITER advanced scenarios [4], as well as to model the RFA plasma response in JET plasmas. This model is based on drift kinetic resonance damping of the mode at relatively low mode frequencies in the plasma frame [5, 6]. In contrast with Refs. [7, 8], we include the kinetic terms self-consistently in the MHD equations, which allows us to compute the kinetic energy perturbation using the RWM eigenfunction modified by drift kinetic effects. In the perturbative approach, the kinetic energy is normally evaluated with eigenfunctions computed for the ideal kink mode without conducting walls. A significant feature of the new model, compared with our previous semi-kinetic model [9, 10, 11], is the full toroidal geometry that we adopt in evaluating the kinetic integrals.

2. Kinetic formulation and benchmarking

We consider the single fluid MHD description of plasmas with a toroidal flow. The core equations,

where the kinetic terms are involved, are written in the Eulerian frame

$$(\gamma + in\Omega)\xi = \mathbf{v} + (\xi \cdot \nabla\Omega)R\hat{\phi}, \quad (1)$$

$$\rho(\gamma + in\Omega)\mathbf{v} = -\nabla \cdot \mathbf{p} + \mathbf{j} \times \mathbf{B} + \mathbf{J} \times \mathbf{Q} - \rho [2\Omega\hat{\mathbf{Z}} \times \mathbf{v} + (\mathbf{v} \cdot \nabla\Omega)R\hat{\phi}], \quad (2)$$

$$(\gamma + in\Omega)\mathbf{Q} = \nabla \times (\mathbf{v} \times \mathbf{B}) + (\mathbf{Q} \cdot \nabla\Omega)R\hat{\phi}, \quad (3)$$

$$(\gamma + in\Omega)p = -\mathbf{v} \cdot \nabla P, \quad (4)$$

$$\mathbf{j} = \nabla \times \mathbf{Q}, \quad (5)$$

$$\mathbf{p} = p\mathbf{I} + p_{\parallel}\hat{\mathbf{b}}\hat{\mathbf{b}} + p_{\perp}(\mathbf{I} - \hat{\mathbf{b}}\hat{\mathbf{b}}), \quad (6)$$

where the variables $\xi, \mathbf{v}, \mathbf{Q}, \mathbf{j}, \mathbf{p}$ represent the plasma displacement, perturbed velocity, magnetic field, current, and pressure tensor, respectively. ρ is the unperturbed plasma density, γ the eigenvalue, n the toroidal mode number, and Ω the plasma rotation frequency along the toroidal angle ϕ . The equilibrium field, current, and pressure are denoted by $\mathbf{B}, \mathbf{J}, \mathbf{P}$, respectively. R is the plasma major radius, $\hat{\mathbf{Z}}$ the unit vector in the vertical direction, \mathbf{I} the unit tensor.

The kinetic terms enter into the MHD equations via the perturbed kinetic pressure tensors shown in Eq. (6), where p is the scalar fluid pressure perturbation, and $p_{\parallel}(\xi_{\perp}), p_{\perp}(\xi_{\perp})$ are the parallel and perpendicular components of the kinetic pressure perturbations, respectively and $\hat{\mathbf{b}} = \mathbf{B}/B, B = |\mathbf{B}|$. The full pressure tensor \mathbf{p} is self-consistently included into the MHD formulation via equation (2).

The perturbed kinetic pressures are calculated from

$$p_{\parallel}e^{-i\omega t + in\phi} = \sum_{e,i} \int d\Gamma M v_{\parallel}^2 f_L^1, \quad p_{\perp}e^{-i\omega t + in\phi} = \sum_{e,i} \int d\Gamma \frac{1}{2} M v_{\perp}^2 f_L^1, \quad (7)$$

where an $\exp(-i\omega t + in\phi)$ -dependence is explicitly assumed for the perturbation, with the mode frequency $\omega \equiv i\gamma$. The integral is carried out over the particle velocity space Γ . M is the particle mass, v_{\parallel}, v_{\perp} are the parallel and perpendicular (to the equilibrium magnetic field) velocity of particle local bounce motion, f_L^1 is the perturbed distribution function defined in the Lagrangian frame and calculated analytically in [5] and [6].

A derivation resulting in a form of p_{\parallel} and p_{\perp} , suitable for numerical implementation, is presented in [12]. A key factor in the kinetic pressure terms is the mode-particle resonance operator

$$\lambda_{ml} = \frac{n[\omega_{*N} + (\hat{\epsilon}_k - 3/2)\omega_{*T} + \omega_E] - \omega}{n\omega_d + [\alpha(m + nq) + l]\omega_b - i\nu_{\text{eff}} - \omega}, \quad (8)$$

where ω_{*N} and ω_{*T} are the diamagnetic drift frequencies due to the density and temperature gradients, respectively. ω_E is the $\mathbf{E} \times \mathbf{B}$ plasma rotation, ω_b the particle transit/bounce frequency, ω_d the bounce-orbit-averaged toroidal precession drift frequency of particles, including the ω_E drift. $\hat{\epsilon}_k = \epsilon_k/T$ is the particle kinetic energy normalised by the temperature. ν_{eff} is the effective collisionality. $\alpha = 1$ for passing particles, and $\alpha = 0$ for trapped particles. m and l are the Fourier harmonic indexes over the poloidal angle and the particle bounce orbit, respectively. The latter implies projecting a time dependent periodic function, associated with the particle periodic bounce motion, on a basis function $\exp(il\omega_b t)$.

Our self-consistent kinetic formulation neglects the perturbed electrostatic potential, the radial excursion of particle trajectory (finite banana width for trapped particles), as well as the FLR corrections to the particle orbit. These effects normally are not important for the RWM. Some of them are crucial to study the kinetic effects on other MHD modes, such as the internal kink mode. Although the formulation is presented for thermal particles, for which a Maxwellian distribution function over the particle energy is assumed, it is relatively easy to extend it to include, for instance, a fast ions contribution or anisotropic distribution functions.

Different from the self-consistent kinetic approach described above, a perturbative approach has been implemented in several codes for studying the kinetic effects on the RWM [7, 8]. In [8], the MHD stability code MISHKA [13] is coupled to the particle orbit-following code HAGIS [14]. The perturbative

approach normally uses the eigenfunction of the ideal kink mode, computed by an ideal MHD code, as the input to further compute the kinetic energy δW_k . The stability of the RWM is then determined by a dispersion relation derived from the kinetic MHD energy principle [15]

$$\gamma\tau_w^* \simeq -\frac{\delta W_\infty + \delta W_k}{\delta W_b + \delta W_k}, \quad (9)$$

where δW_∞ and δW_b are the fluid potential energy without and with a conducting wall, respectively. The fluid energy includes both the plasma and the vacuum contributions. The normalisation factor τ_w^* is related to the wall eddy current decay time. In a cylindrical geometry, $\tau_w^* = \tau_w(1 - b^{-2|m|})/|m|$, with b being the minor radius of the wall, and τ_w defined as the longest eddy current decay time of the wall.

Both perturbative and self-consistent approaches are realised in the kinetic-MHD code MARS-K [12].

Figure 1 compares the growth rates of the $n = 1$ RWM computed by MARS-K and HAGIS, following the perturbative approach. The no-wall ideal kink eigenfunction is used for computing the kinetic integrals. The magnetic precessional drift resonance of trapped thermal ions and electrons with the mode is included in calculations by both codes. A test Solov'ev equilibrium, with aspect ratio of 5 and nearly circular poloidal plasma cross section, is considered. In addition, we assume an equal equilibrium temperature between ions and electrons, as well as uniform radial profiles for the plasma equilibrium density and toroidal rotation ω_E . The latter assumption is equivalent to a finite real mode frequency ω by neglecting the effect of rotation on the ideal kink mode. The dashed line in the figure indicates the growth rate of the fluid RWM without kinetic effects and with no plasma rotation. For this specific equilibrium, the drift kinetic resonances do not provide a significant damping on the mode. Good agreement between MARS-K and HAGIS is obtained. Equally good agreement is achieved under other assumptions (e.g. with ion contribution alone) or for other equilibria.

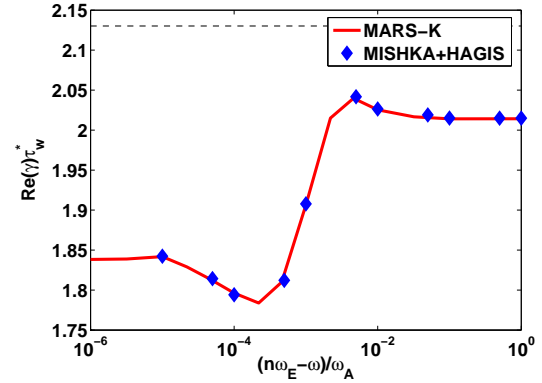


FIG. 1. Comparison of the $n = 1$ RWM growth rates computed by MARS-K and HAGIS, following a perturbative inclusion of the precessional drift resonance damping from trapped thermal particles. A Solov'ev equilibrium is considered with aspect ratio of 5 and nearly circular poloidal plasma cross section. Equal equilibrium temperature for ions and electrons is assumed. Uniform plasma density and rotation profiles are used.

Since the HAGIS code performs a full particle guiding centre orbit integration for the kinetic integrals, the agreement between two codes indicates that neglect of the particle banana width, an assumption made in the MARS-K formulation, is reasonable for such a low frequency mode as the RWM. We point out that, although the benchmark is made on the perturbative approach, it does test the major part of the self-consistent procedure, which relies on the same kinetic integrals as the perturbative approach.

3. Kinetic effects on RWM stability in ITER

We apply MARS-K to investigate the drift kinetic effects on the stability of the RWM for ITER steady state plasmas from Scenario-4 [4]. This scenario has a highly shaped plasma with weak negative magnetic shear at the plasma core. The target plasma, which is marginally unstable to the $n = 1$ ideal external kink mode without a conducting wall, is designed to produce 340 MW fusion power at $Q = 5$. We scale the plasma pressure up to the ideal-wall (inner vacuum vessel) beta limit, while keeping the total plasma current at the design value of 9MA. For the sake of numerical accuracy, we smooth slightly the plasma boundary close to the X-point, without a significant modification of the stability limits. (The no-wall β_N limit is shifted from 2.45 to 2.33, and the ideal-wall limit from 3.65 to 3.62 by smoothing, according to the MARS-F calculations.) Following the convention, we define an equilibrium pressure scaling factor $C_\beta \equiv (\beta_N - \beta_N^{\text{no-wall}})/(\beta_N^{\text{ideal-wall}} - \beta_N^{\text{no-wall}})$, with $C_\beta > 0$ applying above the no-wall limit. All the results reported in this Section are obtained for $C_\beta > 0$.

Figure 2 shows the fluid potential energy of the ideal kink mode (with or without a perfectly conducting wall with the ITER inner wall shape) versus C_β , together with the drift kinetic energy (both real and imaginary parts) computed by MARS-K following the perturbative approach. The kinetic energy comes from the precessional drift resonances of the RWM with trapped thermal ions and electrons (the effect of bounce resonances not being included in this calculation). All the energy is normalised by the plasma inertia, computed using only the displacement perpendicular to the equilibrium magnetic surfaces, of the no-wall ideal kink mode. The ion and electron temperatures are taken equal, which is a reasonable assumption for ITER. The growth rate of the fluid RWM γ_f is used as the complex mode frequency $\omega = i\gamma_f$ in the kinetic integration. We keep the plasma rotation profile as predicted by the ASTRA simulation [4], but vary the rotation amplitude over a wide range. Figure 2 shows an example for a very slow plasma rotation, with the central rotation frequency at 10^{-3} of the Alfvén frequency. The precessional drift resonance is expected to provide the dominant damping at this rotation frequency. The eigenfunction of the no-wall ideal kink mode is used in evaluating the kinetic integrals. We notice a rather large and positive real part of the kinetic energy at relatively small C_β , indicating a strong stabilisation of the mode.

The fluid and kinetic energy perturbations shown in Fig.2 are used to estimate the growth rates of the kinetic RWM, following the dispersion relation (9). The results are shown in Fig.3. The perturbative approach predicts a full kinetic stabilisation of the RWM for a large range of C_β ($0 \leq C_\beta \lesssim 0.8$) at slow plasma rotation. We emphasise that the stabilisation comes solely from the mode resonance with the precession drifts of trapped particles.

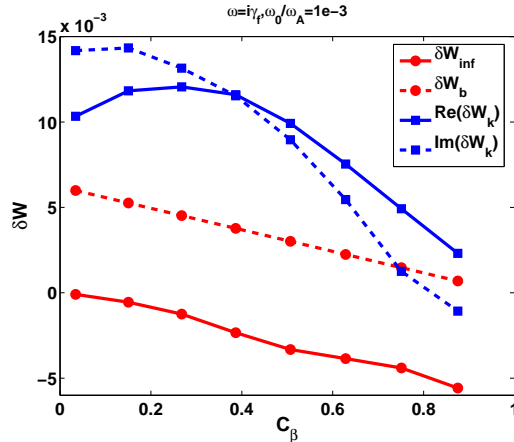


FIG.2. The energy perturbations computed by MARS-K, versus the equilibrium pressure scaling factor C_β for the ITER steady state plasma. Plotted are the fluid potential energy of the ideal kink mode, together with the perturbatively computed kinetic energy from precessional drift resonances of the RWM with trapped thermal particles.

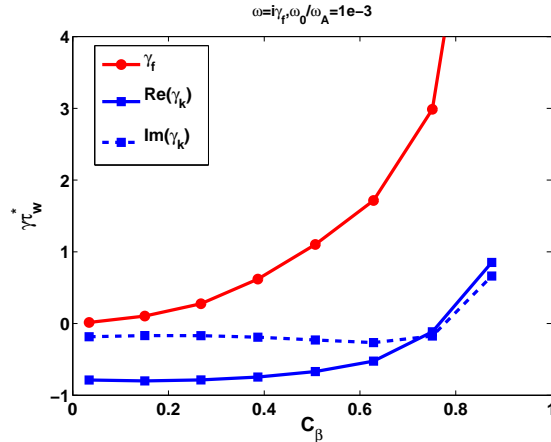


FIG.3. The growth rate of the RWM versus C_β , under the fluid description (γ_f) is compared with that of the kinetic RWM following the perturbative approach (γ_k). Both the growth/damping rate and the real frequency of the kinetic RWM are plotted, for the same ITER plasma as in Fig.2. γ_k is evaluated using formula (9).

For the ITER plasma with relatively slow toroidal rotation, addition of the kinetic contribution from the mode resonance with particle bounce motion does not modify significantly the pictures shown by Fig.2 and 3. As an example, figure 4 compares the MARS-K computed kinetic energy from precessional drift resonance alone, with that from both precessional and bounce resonances. The perturbative approach is followed for an ITER plasma with $C_\beta = 0.5$. The plasma central rotation frequency varies from $2 \times 10^{-4}\omega_A$ to $2 \times 10^{-2}\omega_A$. Figure 5 compares the growth rate of the RWM under the same conditions. The contribution of the bounce resonance damping becomes visible only for the central rotation frequency ω_0 larger than $5 \times 10^{-3}\omega_A$. This contribution almost vanishes for $\omega_0 \lesssim 10^{-3}\omega_A$. The predicted plasma central rotation is less than $2\%\omega_A$ for ITER advanced Scenario-4 [4]. Assuming the rotation profile as predicted for the same ITER plasma, the rotation frequency at the $q = 3$ surface is less than $0.25\%\omega_A$.

(The $q = 2$ surface is absent for this ITER plasma.) The calculation results show that, at the rotation speed predicted for ITER advanced plasmas, the particle bounce resonance damping still plays a minor role. We also notice that the real part of the kinetic energy stays positive (i.e. stabilising) and increases with decreasing rotation frequency, leading to a strong mode suppression at very slow rotation.

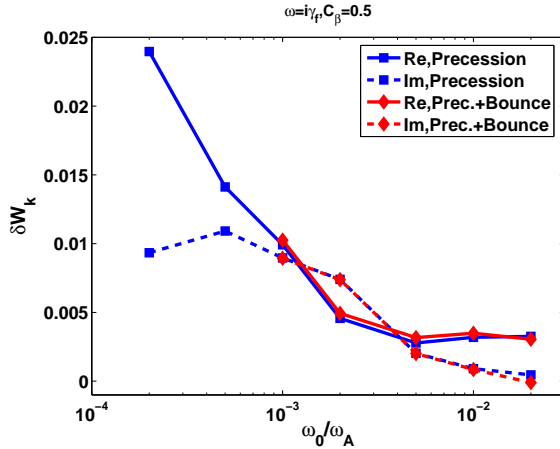


FIG.4. Comparison of the kinetic energy perturbations from precessional drift resonance alone, with that from both precessional and bounce resonances. The perturbative approach is followed for an ITER plasma with $C_\beta = 0.5$. The plasma central rotation frequency varies from $2 \times 10^{-4} \omega_A$ to $2 \times 10^{-2} \omega_A$.

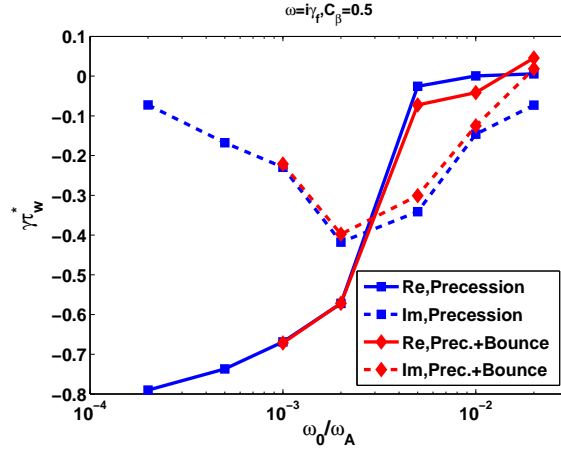


FIG.5. Comparison of the eigenvalue of the kinetic RWM, affected by the precessional drift resonance alone, with that by both precessional and bounce resonances. The perturbative approach is followed for the same ITER plasma as in Fig.4. The plasma central rotation frequency varies from $2 \times 10^{-4} \omega_A$ to $2 \times 10^{-2} \omega_A$.

Figures 6 and 7 compare the 2D plots of the real part of the kinetic RWM eigenvalue, obtained from perturbative and self-consistent approaches respectively. We vary both the plasma pressure and toroidal rotation speed. Due to the different ways of obtaining the mode eigenvalue, the growth/damping is normalised differently between the perturbative and the self-consistent approaches. In the former, the eigenvalue is estimated using the dispersion relation (9), where a normalisation factor τ_w^* is introduced. Strictly speaking, the perturbative approach does not assume any value for the wall time, because the ITER wall resistivity is never involved in the calculations. The self-consistent approach does solve the MHD equations together with the eddy current equations for the resistive walls, hence the wall time τ_w is directly involved. However, at a large enough wall time (i.e. for very highly conducting walls), the plasma inertia becomes negligible, and the mode growth rate is mainly determined by the wall resistivity, hence the normalised growth rate $\gamma \tau_w^*$ is almost independent of τ_w . (In other words, the MARS-K computed γ is inversely proportional to τ_w .) For the ITER equilibrium with $C_\beta = 0.63$, the plasma inertia becomes negligible already at τ_w two orders of magnitude below the true wall time, which is about $6.2 \times 10^5 \tau_A$. For the self-consistent calculations shown in Fig.7, we choose a wall time $\tau_w = 6.2 \times 10^4 \tau_A$, to avoid computing extremely small eigenvalues (in Alfvén units), thus to improve the numerical accuracy. This brings a slight variation to the true growth rate of the kinetic RWM, without modifying the qualitative observations and conclusions made in Fig.7.

Both perturbative and self-consistent approaches predict a full stabilisation of the mode at low pressure ($C_\beta \lesssim 0.4$) and very slow toroidal rotation ($\omega_0/\omega_A \lesssim 2 \times 10^{-3}$), as indicated by the black dots in the figures. However, the perturbative kinetic approach predicts full stabilisation of the mode in a wider range of the $C_\beta - \omega_0$ domain. Using the fluid RWM eigenfunction, instead of an ideal kink, in the perturbative calculations alters figure 6 only slightly. Similar observations have been made in both analytical calculations [16] and numerical tests for other plasma equilibria [12]. The difference in the predicted results has been explained partially by the kinetic modification of the eigenmode structure, and partially by the nonlinear coupling of the RWM eigenvalue via the drift kinetic integrals. For a plasma close to the ideal-wall kink stability limit and with a rotation speed close to the predicted value

for ITER, only partial stabilisation of the RWM is obtained by both approaches.

A similar conclusion is reached in [7] for an ITER like plasma. (The marginally stable ideal kink mode eigenfunctions are used in the perturbative calculations made in [7].) Recent perturbative kinetic simulations for JET plasmas [8] and self-consistent kinetic computations for DIII-D plasmas [17] also confirm the partial stabilisation of the RWM with drift kinetic effects. However, recent experimental results in DIII-D point to a complete stabilisation of the RWM in the linear regime and in the absence of error fields. The latter two conditions, meaning the absence of the RWM coupling to other modes and to the magnetic braking, are assumptions implicitly made in all the above mentioned numerical calculations. In the presence of low level error fields, experiments do observe a finite, but very small critical rotation speed at about $0.3\% \omega_A$ at the $q = 2$ surface [1, 2]. The present kinetic theory offers a close, but not full explanation to the experimental observations. Additional damping physics, such as the one derived from the nonlinear reactive closure in the advanced fluid theory [18], may be considered.

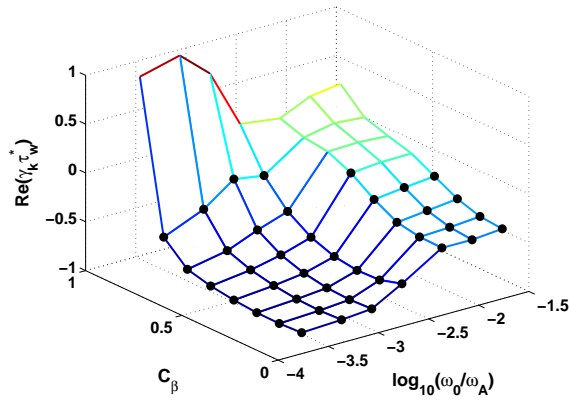


FIG.6. Growth/damping rate of the RWM for ITER advanced tokamak plasmas, predicted by the perturbative kinetic calculations. The precessional resonance damping is included. The black dots indicate a stable RWM.

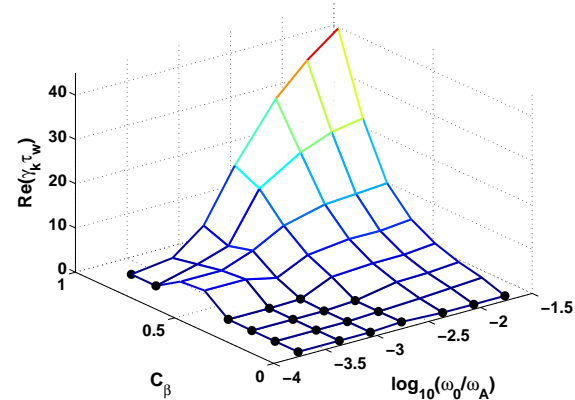


FIG.7. Growth/damping rate of the RWM for ITER advanced tokamak plasmas, predicted by the self-consistent kinetic calculations. The precessional resonance damping is included. The black dots indicate a stable RWM.

4. Kinetic effects on RFA in JET

Figure 8 shows the shapes of the plasma boundary and the JET wall on a poloidal plane. The radial and poloidal location of the error field correction coils (EFCC) and the pick-up coils (close to the wall) are indicated by squares. In the simulation, we allow an infinite number of saddle coils along the toroidal angle ϕ of the torus, in order to generate (or measure) an $\exp(in\phi)$ field pattern, with a single toroidal harmonic n . This is normally not a strong assumption, since 6 saddle coils can generate very well a dominant $n = 1$ field. We note that JET has 4 EFC coils along the toroidal angle, which makes our assumption marginally applicable. The most significant consequence, in comparing the experimental data with the simulation results, is the necessity of mapping out the equivalent $n = 1$ contribution from the experimental total coil current.

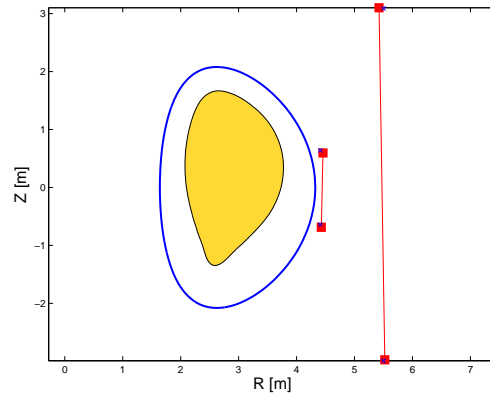


FIG.8. Geometry of the coils used to model the RFA response of the JET plasmas to the EFCC generated external magnetic fields.

The plasma equilibrium is reconstructed from the JET shot 70200. The equilibrium current density does not vanish at the plasma edge, leading to an unstable $n = 1$ peeling mode as the edge q value approaches integer numbers. A toroidal rotation profile, typical for the JET plasmas from the RWM experiments, is considered.

Figure 9 plots the measured RFA amplitude for two similar JET shots 70199 and 70200. The RFA here is defined as the plasma response, measured by the pick-up coils 90° toroidally shifted from the EFCC current, and normalised by the direct vacuum pick-up field in the absence of the plasma. For the JET coil configuration, this quantity measures well the plasma response to the external field. Two peaks occur at β_N values about 2.3 and 2.0, respectively, which are considerably below the estimated no-wall beta limits (about 2.9 and 2.5 respectively). It is unlikely that these two peaks contain a dominant contribution from the response of stable RWM. Besides, experimental evidence suggests a correlation between these low frequency RFA signals and the ELM (edge localised mode) free period prior to the first ELM [19].

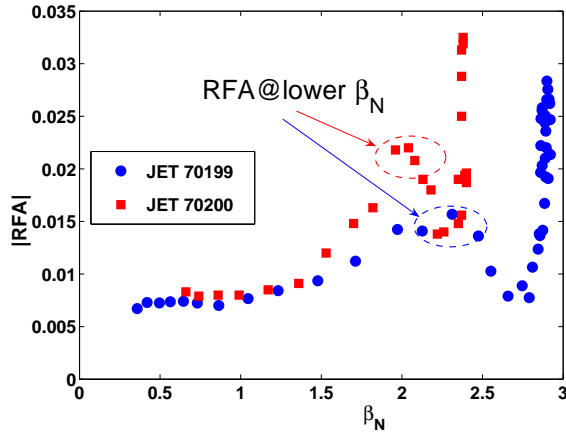


FIG.9. The RFA amplitude measured in two similar JET shots 70199 and 70200, plotted against the normalised plasma pressure. The two peaks occur during the ELM (edge localised mode) events and at beta values considerably below the no-wall limits.

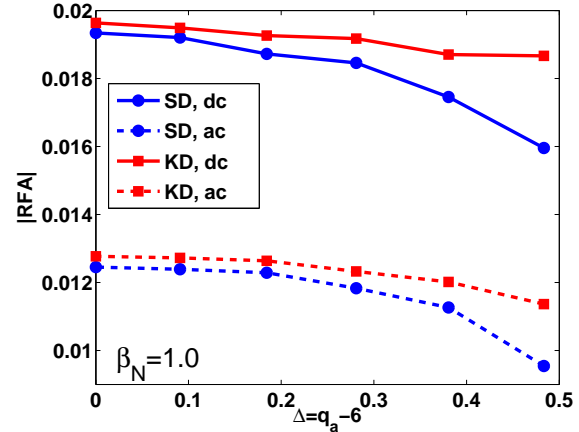


FIG.10. The computed RFA amplitude versus Δ , for a series of JET equilibria reconstructed from shot 70200. Simulations performed with either a strong parallel sound wave damping model (SD), or a toroidal kinetic damping (KD). Static or standing wave EFCC currents are considered.

We explain the two RFA peaks, shown in Fig.9, by the response of marginally stable, $n = 1$ ideal peeling modes. Figure 10 shows the computed RFA amplitude using MARS-K, versus the peeling mode stability parameter Δ , which measures proximity of the edge q value to an integer number. For the JET equilibria considered here, q_a is close to 6, hence $\Delta \equiv q_a - 6$. In the simulation, we vary the total plasma current slightly to scan q_a , keeping a constant low $\beta_N = 1.0$. The equilibrium profiles are also fixed. This allows us to compute the RFA response of the $n = 1$ peeling mode, which is stable as Δ exceeds 0. We expect that the contribution of the stable RWM to the RFA is small at this low β_N value. The calculations are performed with two different damping models in the MARS-K code, namely the parallel sound wave damping [15], and the drift kinetic damping involving the precessional drift resonances of trapped thermal particles. Both static and standing wave (with a frequency equivalent to $1.2 \times 10^{-4} \omega_A$) EFCC currents are assumed. The computed RFA amplitude largely agree with the experimental measurements shown in Fig.9, with the strongest response occurring at $\Delta = 0$, corresponding to a marginally stable peeling mode. The RFA response of the peeling mode is not sensitive to the damping models, in contrary to the RWM, whose stability and response is significantly affected by the mode resonance with plasma particles or waves. We point out that it is difficult to plot the computed RFA together with experimental data, due to the fact that, for a given β_N , the value of Δ , which controls the stability of the peeling mode, depends on the precise details of the equilibrium, especially the current profile at the plasma edge. We also point out that the experimental RFA response, measured near the no-wall beta limit for the ideal external kink mode, is dominantly caused by the stable RWM. This is modelled in detail in Ref. [20].

5. Conclusions

A full toroidal drift kinetic damping model is self-consistently incorporated into the single fluid linear

MHD formulation, via an anisotropic pressure tensor. This approach allows a self-consistent modification of the eigenmode structure and eigenvalue due to kinetic effects. Within the approximations made in this model, it provides a useful tool to study the damping physics of the unstable RWM, as well as the dynamics of a stable RWM.

For ITER steady state advanced scenarios, the self-consistent kinetic model predicts a full stabilisation of the RWM at very slow plasma rotation (less than 0.2% of the Alfvén speed at the plasma centre) and moderately high plasma pressures ($C_\beta \lesssim 0.4$). More optimistic results are obtained by the perturbative approach, where the eigenfunction of ideal kink mode is used to evaluate the kinetic integrals, and an approximate dispersion relation is applied *a-posteriori* for estimating the mode eigenvalue. For a plasma toroidal rotation speed up to the predicted value for ITER, the kinetic damping of the RWM is mainly provided by the precessional drift resonances of trapped thermal particles. In this work, we did not include the kinetic contribution from fast particles. The effect of the plasma collisionality is neglected. A comprehensive prediction of the RWM stability in ITER may require including all these effects, as well as considering even other damping mechanisms.

We apply the drift kinetic damping model to the resonant field amplification in JET plasmas. The RFA response, observed in JET experiments at low plasma pressures (below the no-wall beta limit for an ideal kink), is recovered in simulations, and explained by the response of either a marginally stable, low n ideal peeling mode, and/or the response of an intrinsically stable RWM, whose dynamics is affected by the damping models in combination with the plasma rotation.

Acknowledgements

This work was funded by the United Kingdom Engineering and Physical Sciences Research Council and by the European Communities under the contract of Association between EURATOM and UKAEA. The views and opinions expressed herein do not necessarily reflect those of the European Commission. Work also supported by the US Department of Energy under DE-FG03-956ER54309.

References

- [1] H. Reimerdes, *et al.*, Phys. Rev. Lett. **98**, 055001 (2007).
- [2] E.J. Strait, *et al.*, Phys. Plasmas **14**, 056101 (2007).
- [3] M. Takechi, *et al.* (*JT-60 Team*), Phys. Rev. Lett. **98**, 055002 (2007).
- [4] Polevoi A. *et al.*, Fusion Energy 2002 (Proc. 19th Int. Conf. Lyon, 2002) (Vienna: IAEA) CD-ROM file CT/P-08 and <http://www.iaea.org/programmes/ripc/physics/fec2002/html/fec2002.htm>
- [5] T.M. Antonsen and Y.C. Lee, Phys. Fluids **25**, 132 (1982).
- [6] F. Porcelli, *et al.*, Phys. Plasmas **1**, 470 (1994).
- [7] B. Hu, R. Betti, and J. Manickam, Phys. Plasmas **12**, 057301 (2005).
- [8] I.T. Chapman, *et al.*, “Kinetic Effects on the Resistive Wall Mode”, Plasma Phys. Control. Fusion, submitted (2008).
- [9] A. Bondeson and M.S. Chu, Phys. Plasmas **3**, 3013 (1996).
- [10] Yueqiang Liu, *et al.*, Nucl. Fusion **44**, 232 (2004).
- [11] Y.Q. Liu, *et al.*, Nucl. Fusion **45**, 1131 (2005).
- [12] Yueqiang Liu, *et al.*, “Toroidal self-consistent modelling of drift kinetic effects on the resistive wall mode”, Phys. Plasmas, submitted (2008).
- [13] A.B. Mikhailovskii, *et al.*, Plasma Phys. Rep. **23**, 844 (1997).
- [14] S.D. Pinches, *et al.*, Comput. Phys. Commun. **111**, 133 (1998).
- [15] M.S. Chu, *et al.*, Phys. Plasmas **2**, 2236 (1995).
- [16] Yueqiang Liu, *et al.*, Phys. Plasmas **15**, 092505 (2008).
- [17] Yueqiang Liu, *et al.*, B12, Invited talk at 50th APS-DPP Annual Meeting, November 17-21, 2008, Dallas, Texas, to be submitted to Phys. Plasmas.
- [18] J. Weiland, private communications (2007).
- [19] M.P. Gryaznevich, *et al.*, “Experimental Studies of Stability and Beta Limit in JET”, Proc. 35th EPS Conference on Control. Fusion and Plasma Phys. (Crete, Greece, 2008), ECA 32A I3-044.
- [20] Yueqiang Liu, *et al.*, “Modelling of resonant field amplification due to low- n ideal MHD modes in JET”, Plasma Phys. Control. Fusion, submitted (2008).